Saudi Journal of Biological Sciences 28 (2021) 1226–1232

Contents lists available at ScienceDirect

Saudi Journal of Biological Sciences

journal homepage: www.sciencedirect.com

Original article

Mathematical modeling and experimental analysis of the efficacy of photodynamic therapy in conjunction with photo thermal therapy and PEG-coated Au-doped TiO_2 nanostructures to target MCF-7 cancerous cells

Seemab Iqbal [a], M. Fakhar-e-Alam [a,*], K.S. Alimgeer [b], M. Atif [c], Atif Hanif [d], Nafeesah Yaqub [c], W.A. Farooq [c], Shafiq Ahmad [e], Yu-Ming Chu [f,g,*], Muhammad Suleman Rana [h], Amanullah Fatehmulla [c], Hijaz Ahmad [i,j]

[a] Department of Physics Govt. College University, 38000, Faisalabad, Pakistan
[b] Department of Electrical and Computer Engineering, COMSATS University, Islamabad, Islamabad campus, Pakistan
[c] Department of Physics and Astronomy, College of Science, King Saud University, Riyadh 11451, Saudi Arabia
[d] Botany and Microbiology Department, College of Science, King Saud University, Riyadh 11451, Saudi Arabia
[e] Industrial Engineering Department, College of Engineering, King Saud University, P.O. Box 800, Riyadh 11421, Saudi Arabia
[f] Department of Mathematics, Huzhou University, Huzhou 313000, China
[g] Hunan Provincial Key Laboratory of Mathematical Modeling and Analysis in Engineering, Changasha, University of Science & Technology, Changsha 410114, China
[h] National Institute of Health, Islamabad, Pakistan
[i] Department of Basic Sciences, University of Engineering and Technology, Peshawar 25000, Pakistan
[j] Section of Mathematics, International Telematic University Uninettuno, Corso Vittorio Emanuele II, 39, 00186 Roma, Italy

ARTICLE INFO

Article history:
Received 10 November 2020
Revised 25 November 2020
Accepted 30 November 2020
Available online 8 December 2020

Keywords:
PEG-coated Au-doped Titanium oxide (TiO_2) nanostructures
Photodynamic therapy (PDT)
Photothermal therapy/(HET)
MCF-7 cancerous cells

ABSTRACT

Some nanoscale morphologies of titanium oxide nanostructures blend with gold nanoparticles and act as satellites and targeted weapon methodologies in biomedical applications. Simultaneously, titanium oxide can play an important role when combined with gold after blending with polyethylene glycol (PEG). Our experimental approach is novel with respect to the plasmonic role of metal nanoparticles as an efficient PDT drug. The current experimental strategy floats the comprehensive and facile way of experimental strategy on the critical influence that titanium with gold nanoparticles used as novel photosensitizing agents after significant biodistribution of proposed nanostructures toward targeted site. In addition, different morphologies of PEG-coated Au-doped titanium nanostructures were shown to provide various therapeutic effects due to a wide range of electromagnetic field development. This confirms a significantly amplified population of hot electron generation adjacent to the interface between Au and TiO_2 nanostructures, leading to maximum cancerous cell injury in the MCF-7 cell line. The experimental results were confirmed by applying a least squares fit math model which verified our results with 99% goodness of fit. These results can pave the way for comprehensive rational designs for satisfactory response of performance phototherapeutic model mechanisms along with new horizons of photothermal therapy (HET) and photodynamic therapy (HET) operating under visible and near-infrared (NIR) light.

1. Introduction

Since the discovery of its tremendous photocatalytic performance in water splitting under ultraviolet (UV) light, titanium dioxide (TiO_2) has garnered significant attention (Fujishima et al., 2008; Chen and Selloni, 2014; Zhang et al., 2014). Comprehensive research on the fabrication, structure, and applications of TiO_2 nanostructures (Devi and Kavitha, 2013; Dozzi and Selli, 2013; Xu et al., 2014) have been carried out. The functionalization of TiO_2 nanostructured materials has been applied to nanobiotechnology in drug delivery systems, photothermal therapy, bone scaffolds, vascular stents, and biosensors. Recently, nano-TiO_2 scaffolds have been shown to increase the speed of apatite formation

Abbreviations: NRA, Neutral red assay; PEG, Polyethylene glycol; RMSE, Root mean square error; SPR, Surface plasmon resonance; TEM, Transmission electron microscope.

* Corresponding authors at: Department of Mathematics, Huzhou University, Huzhou 313000, China (Y. Chu).
E-mail addresses: fakharphy@gmail.com (M. Fakhar-e-Alam), chuyuming2005@126.com (Y.-M. Chu), hijaz555@gmail.com (H. Ahmad).

Peer review under responsibility of King Saud University.

Production and hosting by Elsevier

https://doi.org/10.1016/j.sjbs.2020.11.086
1319-562X/

and enhance cell adhesion, proliferation, and differentiation. (Primo etal.,2011;Cushingetal.,2012,2015;Lietal.,2015;Mubeenetal.,2013).

Similarly, gold nanomaterials (Au NMTs) have proven to be useful in the field of medical nanotechnology by providing light at the nanoscale and being incorporated into biological systems (Govorov et al., 2013; Furube et al., 2007). Most of these applications are based on an optical phenomenon such as localized surface plasmon resonance, which is highly tunable by the size and morphology of the nanoparticle (Daniel and Astruc, 2004). It can be regulated to specifically absorb or scatter light at specific wavelengths between the visible and near-infrared (NIR) range of the light spectrum. For maximum penetration in the visible-NIR range for therapeutic tissue, NIR is the most appropriate region. Compared with conventional therapeutic materials, gold nanostructures provide several advantages for biomedical applications, including high biocompatibility and non-cytotoxicity toward healthy tissues, passive accumulation at tumor sites due to enhanced permeability and retention effects (Liz-Marzán, 2006; Kochuveedu et al., 2012), and ease of bioconjugation via Au-TiO_2 bonding to provide increased stability and active tumor targeting at the nanoscale (Oros-Ruiz et al., 2011; Murdoch et al., 2011). Metal nanoparticles and hybrid metal/TiO_2 have been utilized in the development of new band gaps suitable for cancer therapy and other relevant applications. In addition, due to the significant research contributions of gold embedded with TiO_2, the hybrid form has become renowned in biosensors, optical sensors (Li et al., 2015; Hu et al., 2014; Kodiyath et al., 2014; Alvarez-Puebla et al., 2010), and absorption components in solar cells and gas sensing systems (Stöber et al., 1968).

Most applications utilizing optical resonances in the visible region of the electromagnetic spectrum are due to surface plasmon resonance (SPR) absorption. NP dispersion depends on plasmon resonance frequency, while this frequency depends on size, morphology, shape, and distribution, as well as the particular dielectric characteristics of the surrounding dispersion medium (Sclafani and Herrmann, 1996; Xu et al., 2011). Consequently, oscillations induced by electromagnetic radiation on the conductive surface electrons of the nanoparticles can alter the position and intensity of the SPR with changes in volume fraction, size and morphology of the grown novel nanoparticles. Furthermore, particle interaction dependency may occur for high densities of nanostructure volume fraction ($\geq$17%), and red shifting of SPR was detected with increasing particle size (Zuber et al., 2016). For dielectric media doping, milieu and ion implantation via manifold process are essential. Also, doping with magnetic and other transition metals to extend the technology has been the subject of research over the past few years (Kaur et al., 2018; Tedstone et al., 2016; He et al., 2018).

Simple and common superficial synthetic methods can be adopted due to the outstanding colloidal stability of these nanostructures. For the purpose of electron plasmonic response and electrochemical response of Au interfaces with TiO_2 hybrid hierarchical architectures consisting of various morphologies, the process must be controlled via synthesis (concentration, temperature, irradiation time etc.), which allows for better understanding of this innovative strategy. Moreover, the numerical simulation response of the electron injection mechanism from gold to TiO_2 has been uncovered. In this work, the mechanism of energy band gap electron transfer has been explored.

2. Materials and methods

2.1. 1. Synthesis procedure of titanium oxide nanoparticles

Titanium butoxide, oleic acid, oleyl amine, and absolute ethanol were purchased from Sigma Aldrich chemicals. TiO_2 nanospheres were synthesized by a sol gel method. In this composition, titanium butoxide, (4.5 g), oleic acid (90%) (4.5 g), oleyl amine (80–90%) (4.3 g), and absolute ethanol (3.3 g) were added into a beaker and sonicated for few minutes. Then, the mixture was stirred for 20 min. The aqueous solution was poured into a hydrothermal Teflon reactor and 4 mL of DI water and 10 mL of ethanol were added into the empty space of the autoclave lining. The vessel was placed into a furnace at 200 ^{0}C for 24 h until a white precipitate of titanium nanoparticles formed. The nanoparticles were then washed twice with ethanol in a centrifuge at 11000 rpm for 10 min at room temperature. Particle dispersions were achieved by adding 95% n-hexane C_6H_{14}, and a non-polar chain was attained by mixing in cyclohexane C_6H_{12}. Each mixture was stored at room temperature until the white precipitate settled.

2.1.1. Deposition of gold nanostructures on TiO_2 nanoparticles

By adopting the seed growth mechanism, various morphologies of gold nanostructures were preferred using various ratios of benzyl-hexadecyl trimethyl ammonium chloride and CTAB. Using this simple technique, the gold content of the growth solution was used to grow NRs of ultrafine structures by adopting the same seed growth procedure as attempted by Babak Nikoobakht (Lkhagvadulam et al., 2013).

2.1.1.1. Capping polyethylene glycol (PEG) –Co- Au-doped TiO2 nanostructures. 350 mg of PEG (200 μmol of PEG-2000) was added into 85 mL of Au-doped TiO_2 nanostructures for 4 to 5 h of vigorous stirring at room temperature. After the reaction was completed, the final product was frozen and dried. This form could be analyzed with various techniques. The fabrication of TiO_2 nanostructures with Au hierarchy is presented in Fig. 1. Fig. 1 (a) describes the schematic of Au nanospheres capped on the TiO_2 nanostructure. Fig. 1(b) illustrates the schematic of Au nanorods capped on the TiO_2 nanostructure, and Fig. 1(c) describes the PEG-coated Au nanospheres capped on the TiO_2 nanostructure. Fig. 1(d) describes the schematic of PEG-coated Au nanorods capped on TiO_2 nanostructure Fig. 1(e) depicts the newly developed band gap of PEG-capped Au-doped TiO_2, and the corresponding hot electron generation enhancement in the Fermi sea of Au-doped TiO_2 nanostructures. The concept of the mutual effect of hot electrons/PTT and PDT is novel. As long as the concentration of PEG-coated Au-doped titania increases, the loss in cell viability significantly decreases which is an indication of remarkable drug delivery toward a targeted cancerous site.

2.2. Cell culturing of MCF-7 cell line and labeling for PEG-coated Au-doped TiO_2 nanostructures

The MCF-7 cell line (breast carcinoma) was individually cultured in 25 cm^2 plastic tissue flasks. The flasks contained a minimum essential medium with bicarbonate ions (Hanks salts), 10% FBS, and 2 mM glutamine along with nonessential amino acids. The cells were incubated for 48 h to allow the cells to stick to the flask and controlled parameters were maintained at 37 °C in moist air. The 70–80% seeded cells were harvested by 0.25% trypsin. The breast carcinoma cells culture and 96-well plates containing 2% fetal bovine serum were used in the presence of 5% CO_2 0–400 μg/mL of a dispersed solution of PEG-coated Au-doped TiO_2 nanostructures added to each row of the 96-well plates for hot electron therapy and PDT analysis (Atif et al., 2019).

2.3. PDT of PEG-coated Au-doped TiO_2 nanostructures

Photodynamic efficacy of the nanoparticles was conducted after suitable irradiation at the optimal wavelength of light and exposure of PEG-coated AuNP-coated TiO_2 nanoparticles into MCF-7 cells by optimizing incubation time (0–200 min). In these experi-

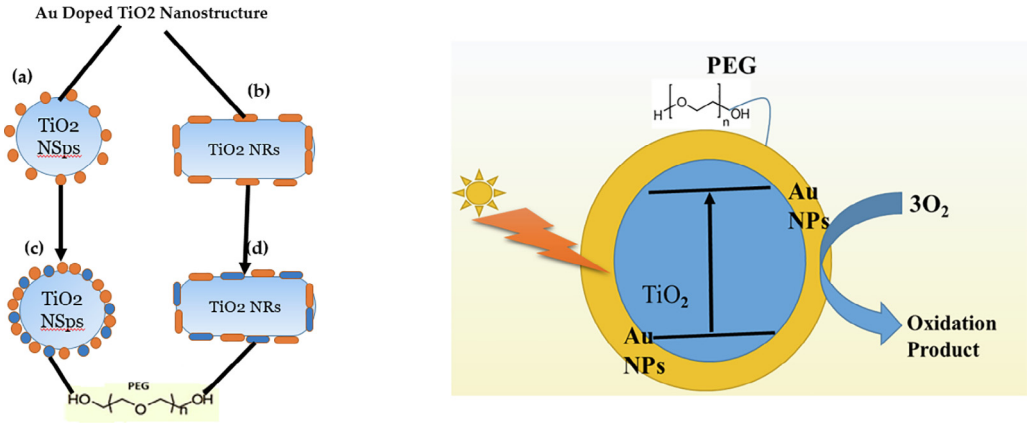

Fig. 1. Illustration of the deposition of (a) Au nanospheres doped TiO_2 nanostructures; (b) Au nanorods doped TiO_2 nanostructure; (c) PEG-coated Au nanospheres doped TiO_2 nanostructure; (d) PEG-coated Au nanorods doped TiO_2 nanostructure; (e) Photoexcitation mechanism of PEG coated Au doped TiO_2 nanostructure after laser exposure.

ments, UV contributions were screened out, and the degree of TiO_2 photosensitization was confirmed. The 96-well plates were arranged in eight columns, and each column contained 4 wells. The final two columns were used as standards. Moreover, 100–400 μg/mL of a dispersed solution of PEG-coated Au-doped TiO_2 nanoparticles were added to each row of the 96-well plates for hot electron therapy and PDT analysis. The incubation time was fixed for 0–200 min. The PEG-coated Au-doped TiO_2 nanoparticles uptake was recorded. The neutral red assay (NRA) is a conventional procedure that precisely determines cell viability by using a microplate reader. Various PDTs were performed after preparing and labeling of solutions of different concentrations of PEG-coated Au-doped TiO_2 into the MCF-7 cellular model (Iqbal et al., 2019a, 2019b).

2.4. NRA assessment of peg-coated-au-doped TiO2 nanostructures

The NRA is a conventional procedure that precisely determines cell viability by using a microplate reader. Various PDT optimized parameters were performed after preparing and labeling solutions of different concentrations of PEG-co-Au-doped TiO_2 nanostructures into the MCF-7 cellular model. In the first step, the cells were seeded in 96-well plates and exposed to different concentrations of dispersed PEG-co-Au-doped TiO_2 nanostructures in the absence and presence of laser light exposure (UV light (200 nm to 240 nm of light wavelength) and visible region of light (630 nm of wavelength)). After 24 h of cell incubation with PEG-co-Au-doped TiO_2 nanostructures at an optimal concentration, 50 μL of NRA (50 mg/mL) was incorporated in the treated cultured plate and incubated for 3 h (Fakhar-e-Alam et al., 2020). The medium was removed and the cells were washed with 40% formaldehyde and 10% $CaCl_2$ (*v*/*v*, 4:1). In the next step, a complex of 45% ethanol and 15% acetic acid (1:1) was assimilated to extract NR. In a further step, the NR-mixed plate was shaken and kept free for 15 min. The absorbance was then examined at 510 nm. The quantification of solubilized dye was statistically analyzed with the living cell numbers according to the % cell viability formula (Iqbal et al., 2019). Solution uptake/absorbance was assessed by selecting a filter compatible with the microplate reader.

3. Results

3.1. Material characterization of PEG-coated Au-doped TiO_2 nanostructures

We have carried out the fundamental concept of PEG-coated gold-titanium nanostructures for treatment via hot electron therapy/photo thermal therapy. Optimizing the Au-doped TiO_2 nanostructures with respect to morphology, size, optical absorption band, and purity is a major challenge. The surface morphology of the prepared composites was analyzed by a JEM 1230 transmission electron microscope (TEM).

3.2. Morphology analysis

The morphology of TiO_2 nanospheres and Au-doped TiO_2 nanospheres were confirmed using TEM, as depicted in Fig. 2. TEM images confirmed immobilization and homogeneous distribution of the nanospheres (5–10 nm) and nanorods (15–20 nm) respectively.

3.3. PDT combined with HET of MCF-7 cells exposed with nanostructures

A boosted form of the effective injection of generated hot electrons via photothermal therapy across the Schottky barrier to the conduction band of TiO_2 triggers the formation of excitons and the successive liberation of essential radical species which is beneficial toward reactive oxygen species liberation which leads to cell death (Fakhar-e-Alam et al., 2020). Even though the peak intensity of the indigenous fields created by the surface plasmon exponentially decay with distance, the contact between the Au and TiO_2 allows for an efficient interaction between both components. In addition, the robust scattering of Au NSTs may lead to enhanced optical concentration and thus, an enhanced light absorption of TiO_2 (Kovacs et al., 2015). Fig. 3 shows cell viability graph of MCF-7 vells exposed with Gold doped Titania and PEG coated Gold doped Titania. Fig. 4 shows percentage cell viability graph of MCF-7 Cells after treatment with PDT and PDT along HET.

3.4. Mathematical modeling

Data was obtained from experimental studies by varying the concentration (μg/mL) of nanostructures and measuring the % cell viability. The experiment was repeated for Au-doped titania μg/mL, PEG-coated Au-doped titania μg/mL, PDT only, and PDT + HET (combined therapy effect) and the data is shown in Tables 1. Then, a mathematical model was used to fit the data (Iqbal et al., 2019a, 2019b). It was proposed to have a bi-exponential model as presented in equation 1 by observing the nature of the data with respect to the increasing concentration (Fakhar-e-Alam et al., 2020; Iqbal et al., 2019).

$$f(x) = ae^{bx} + ce^{dx} \text{ (eq 1)}$$

The careful selection of a mathematical function able to accurately represent the data was based on various parameters of good-

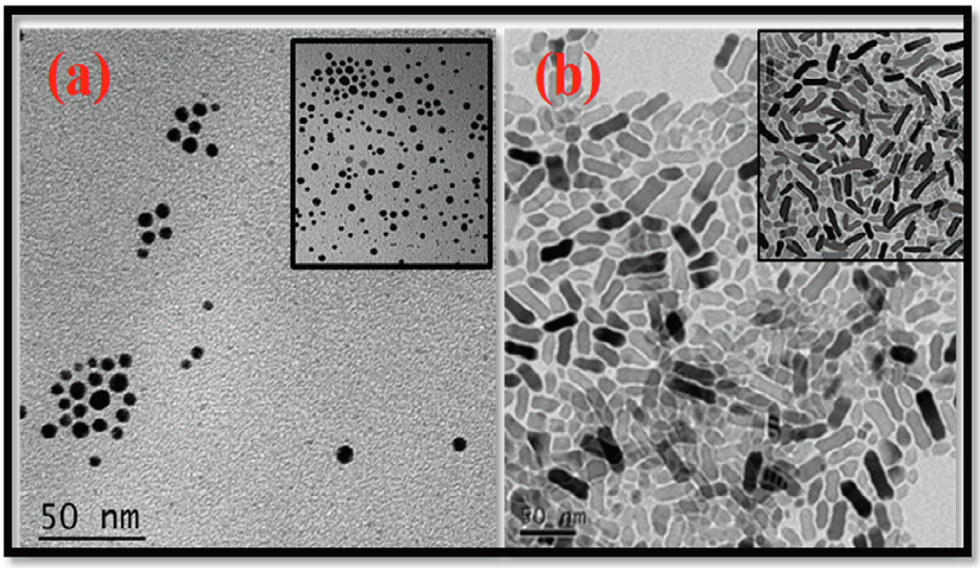

Fig. 2. TEM images of differently shaped PEG-coated Au-doped TiO_2 nanostructures (a) nanospheres (b) nanorods.

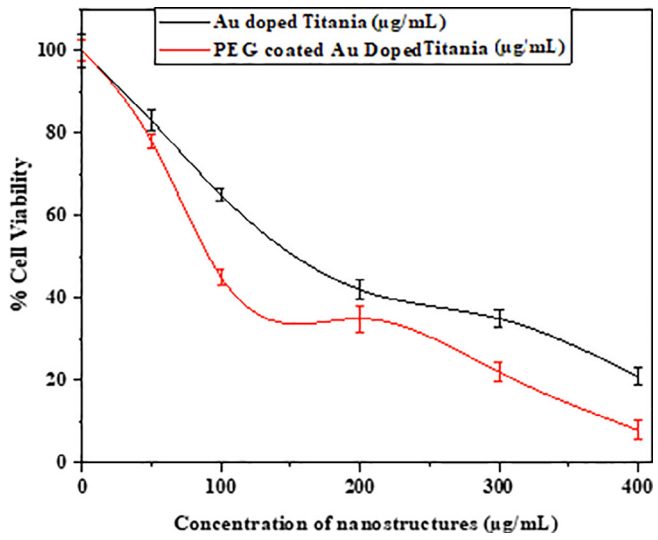

Fig. 3. Cell viability graph of MCF-7 cells exposed with gold-doped Titania and PEG-coated gold-doped Titania.

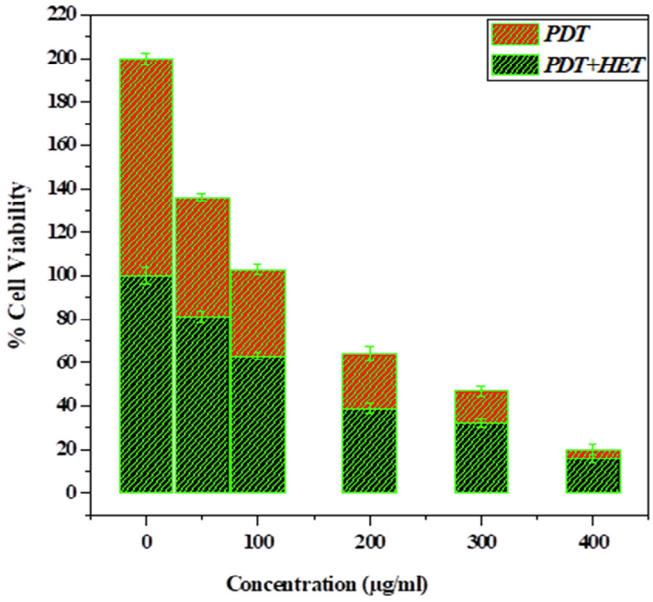

Fig. 4. %Cell Viability graph of MCF-7 Cells after treatment with PDT and PDT along HET.

ness of fit like SSE, R-squared values, adjusted R-squared values, and root mean square error (RMSE). Other functions are likely to present poor values for goodness of fit. Moreover, having a bi-exponential model for representation of all the experiments had provided ease of finding out the best therapy and a quantitative benchmark in general. Therefore, using equation 1 shows a comparison for which therapy is better for the patient (Fig. 5) (Xu et al., 2007).

It can be observed that "*b*" and "*d*" are coefficients representing the decay constant in the bi-exponential model. The values of "*b*" are more important and play a vital role in deciding the decay factor and, hence, the shape of the tapering at lower values of concentration, while the negative sign shows that % cell viability decreases with increasing concentration (µg/mL) (Fig. 6).

4. Discussion

Experimentally, titania nanospheres (~200 nm) were successfully synthesized and by applying a controlled chemical reaction, various nanomorphologies of Au nanostructures were generated on the surface of the 200 nm-nanosphere of TiO_2. PEG was encapsulated on the surface of the Au composite TiO_2 nanospheres after the final layer. In this experiment, the role of the outer layer of organic material (PEG) was significant relative to stability and valuable nanomaterial delivery through delicate blood vessels. From the TEM image, it is obvious that Au nanostructures retain their structural integrity throughout the assembly process, and the crystalline nature of the TiO_2 inner layer was confirmed by HRTEM analysis. HRTEM images (lower panel of Fig. 2) clearly showed that Au dopant was well distributed and decorated on the surface of host TiO_2 NPs. High resolution TEM images also demonstrated that TiO_2 NPs are highly crystalline, which matches well with the (101) plane of powdered TiO_2 (Moosavi et al., 2016; Tisdale et al., 2010).

The random morphology of the Au nanostructures was oriented into solution and photo energy production was shown to be dependent on size, shape, and anisotropy of the nanomaterial.

Table 1
Estimation of constants used in equation 1 based on the least square error method, along with goodness of fit parameters.

	a	*b*	*c*	*d*	SSE	R-square	Adjusted R-square	RMSE
Au	47	−0.00665	53.75	−0.00256	28.17	0.9939	0.9847	3.753
PEG	26.42	−0.01464	74.76	−0.004614	143.3	0.9763	0.9409	8.464
PDT	99.28	−0.004266	−1.8e-15	0.08659	34.55	0.9932	0.983	4.157
PDT + HET	28.41	−0.0701	71.59	−0.005605	19.4	0.9968	0.9919	3.114

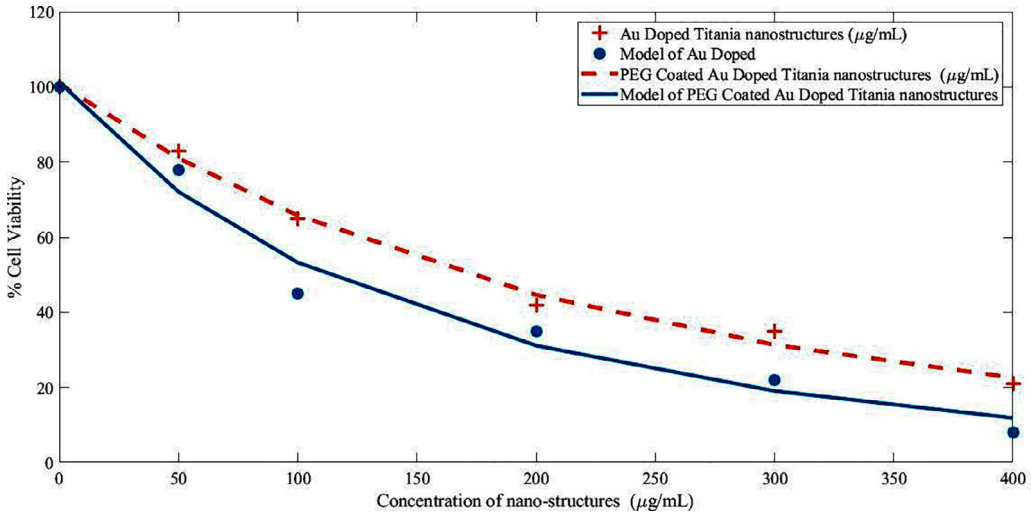

Fig. 5. Modeling of %cell viability graph of MCF-7 cells exposed with gold-doped titania and PEG-coated gold-doped titania nanostructures.

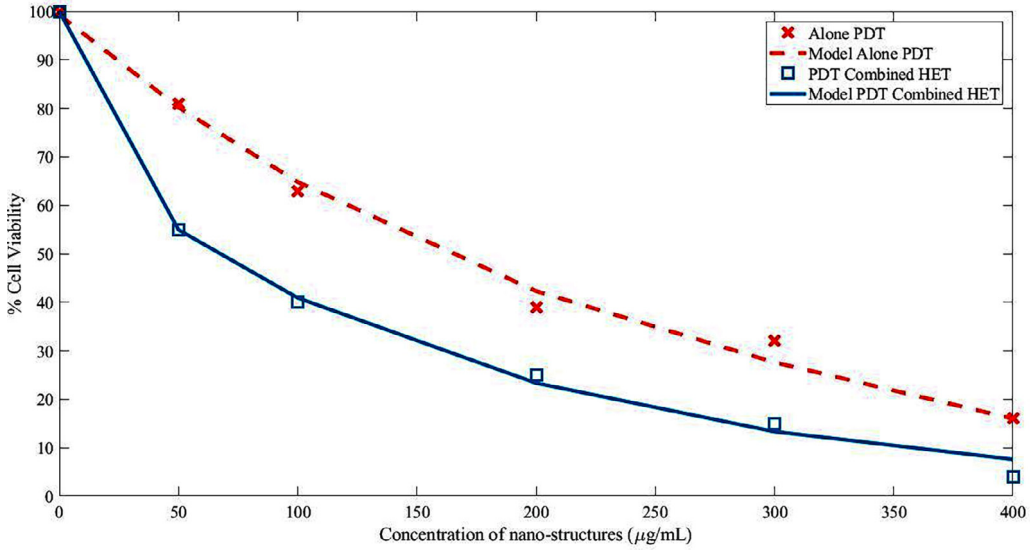

Fig. 6. Modeling of %cell viability graph of MCF-7 cells after treatment with PDT and PDT along HET.

Cell viability loss in MCF-7 cells were employed by exposing with individual Au-doped titanium nanomorphology and PEG-capsulated gold-doped titania in Fig. 3. The concept of mutual effect of hot electrons and PDT is novel (Clavero, 2014; Qiu et al., 2018). As long as the concentration of PEG-coated Au-doped titania increases, the loss in cell viability will significantly decrease which is indicative of remarkable drug delivery toward targeted/cancerous site. This has been observed after Au-doped titania NSTs formation with and without PEG, and the biodistribution results were compared. Beyond 100 μg/mL NPs concentration, significant loss in cell viability was assessed, which is about 79% in the cases of gold and TiO_2 nanostructures at 400 μg/mL, and this loss reaches 92% at PEG-coated gold nanostructures with TiO_2 at 400 μg/mL. Similar therapeutic studies were conducted toward a malignant cell model (Atif et al., 2020, 2016).

The aim of our experimental approach was to discriminate the possibility of individual and mutual effect of photothermal therapy and photodynamic therapy. It had been evaluated that the absorption spectra of gold lied in the region of 525 nm 560 nm, as long as the size of Au NSTs increases the absorption peak shifted to longer wavelengths. However, for Au-doped titania, two types of therapies were noted in the case of PEG-coated Au-doped titania under

525 nm and (525 and 560 nm) of light wavelength. It was determined that terms of only 525 nm of red-light exposure toward PEG-coated Au-doped TiO_2 exposed MCF-7 breast cancer cells, only photodynamic therapy effects were recorded as depicted in Fig. 3 (Atif et al., 2016). Because of this, the cell viability loss went from 50% to 90% when NPs were exposed to 100 μg/mL to 400 μg/mL of PEG-coated Au-doped TiO_2, respectively. Although, in the case of two wavelength laser additions in a single shot (525 and 560 nm), PDT and photothermal therapy were confirmed. In the case of the combined effects of PDT with HET, ~98% loss in cell viability were measured, which is quite significant and was confirmed by applying multiple reliable tests, as shown in Figs. 4 and 5.

The combination of photodynamic therapy and photothermal therapy (PDT and HET) plays a vital role in the successful treatment of cancer patients, and these experimental results have validated this novel achievement. It was further observed that the value of "*b*" is highest for PDT + HET (Fig. 6), which clearly indicated this as the optimal therapy compared to others listed in the table. The model also showed excellent goodness of fit values of R-squared, Adjusted R-squared, RMSE, and SSE (Iqbal et al., 2020). In summary, this novel form has 98.5% malignant cell killing potential as confirmed by experimental data.

5. Conclusions

We have demonstrated the role of gold-doped titania (Au-doped TiO_2) toward biomedical applications. It was shown that the morphology of Au on the titania surface played a significant role in the efficacy of the combined photothermal and photodynamic therapies. The morphology and crystallite of different hybrid forms were confirmed by applying TEM. In addition, problems of drug uptake resistance and drug release were advocated by incorporating the PEGylated form of gold-doped TiO_2 which showed enhanced quantities of ligands toward the targeted site.

In this article, a new strategy of hot electron generation synergistic coupling with powerful PDT treatment modality was introduced toward the vitro/MCF-7 model. It was concluded that this synergistic approach toward malignant cell killing potential up to 98.5% was confirmed by experimental data analysis. In the light of current experimental findings, it is expected that in the near future, this combined therapeutic effect will be preferable over all traditional/conventional techniques. Additionally, the experimental results agreed well with a least squares fit math model.

Declaration of Competing Interest

The authors declare that they have no known competing financial interests or personal relationships that could have appeared to influence the work reported in this paper.

Acknowledgement

The authors extend their appreciation to the Deanship of Scientific Research at King Saud University for funding this work through research group number RGP-293. The author would like to specially thank the Higher Education Commission (HEC) Pakistan for the financial support under NRPU Grant No. 8056/Punjab/NRPU/R&D/HEC/ 2017. The research was supported by the National Natural Science Foundation of China (Grant Nos. 11971142, 11871202, 61673169, 11701176, 11626101, 11601485).

References

Fujishima, A., Zhang, X., Tryk, D.A., 2008. TiO2 photocatalysis and related surface phenomena. Surf. Sci. Rep. 63, 515–582. https://doi.org/10.1016/j.surfrep.2008.10.001.

Chen, X., Selloni, A., 2014. Introduction: titanium dioxide (TiO2) nanomaterials. Chem. Rev. 114, 9281–9282. https://doi.org/10.1021/cr500422r.

Zhang, G., Kim, G., Choi, W., 2014. Visible light driven photocatalysis mediated via ligand-to-metal charge transfer (LMCT): an alternative approach to solar activation of Titania. Energy Environ. Sci. 7, 954–966. https://doi.org/10.1039/c3ee43147a.

Devi, L.G., Kavitha, R., 2013. A review on Nonmetal ion doped Titania for the photocatalytic degradation of organic pollutants under UV/solar Light: role of photogenerated charge carrier dynamics in enhancing the activity. Appl. Catal. B. 140–141 (559–587), 559–587. https://doi.org/10.1016/j.apcatb.2013.04.035.

Dozzi, M.V., Selli, E., 2013. Doping TiO2 with P-block elements: effects on photocatalytic activity. J. Photochem. Photobiol. C. 14, 13–28. https://doi.org/10.1016/j.jphotochemrev.2012.09.002.

Xu, H., Ouyang, S., Liu, L., Reunchan, P., Umezawa, N., Ye, J., 2014. Recent advances in TiO_2-based photocatalysis. J. Mater. Chem. A. 2, 12642–12661. https://doi.org/10.1039/C4TA00941J.

Primo, A., Corma, A., García, H.T., 2011. Titania Supported gold nanoparticles as photocatalyst. Phys. Chem. Chem. Phys. 13, 886–910. https://doi.org/10.1039/C0CP00917B.

Cushing, S.K., Li, J., Meng, F., Senty, T.R., Suri, S., Zhi, M., Li, M., Bristow, A.D., Wu, N., 2012. Photocatalytic activity enhanced by plasmonic resonant energy transfer from metal to semiconductor. J. Am. Chem. Soc. 134, 15033–15041. https://doi.org/10.1021/ja305603t.

Cushing, S.K., Li, J., Bright, J., Yost, B.T., Zheng, P., Bristow, A.D., Wu, N., 2015. Controlling plasmon-induced resonance energy transfer and hot electron injection processes in Metal@TiO2 core–shell nanoparticles. J. Phys. Chem. C. 119, 16239–16244. https://doi.org/10.1021/acs.jpcc.5b03955.

Li, J., Cushing, S.K., Meng, F., Senty, T.R., Bristow, A.D., Wu, N., 2015. Plasmon-induced resonance energy transfer for solar energy conversion. Nat. Phot. 9, 601–607. https://doi.org/10.1038/nphoton.2015.142.

Mubeen, S., Lee, J., Singh, N., Krämer, S., Stucky, G.D., Moskovits, M., 2013. An autonomous photosynthetic device in which all charge carriers derive from surface plasmons. Nat. Nano. 8, 247–251. https://doi.org/10.1038/nnano.2013.18.

Govorov, A.O., Zhang, H., Gun'ko, Y.K., 2013. Y. K Theory of photoinjection of hot plasmonic carriers from metal nanostructures into semiconductors and surface molecules. J. Phys. Chem. C. 117, 16616–16631. DOI: 10.1021/jp405430m.

Furube, A., Du, L., Hara, K., Katoh, R., Tachiya, M., 2007. Ultrafast plasmon-induced electron transfer from gold nanodots into TiO2 nanoparticles. J. Am. Chem. Soc. 129, 14852–14853. https://doi.org/10.1021/ja076134v.

Daniel, M.C., Astruc, D., 2004. Gold nanoparticles: assembly, supramolecular chemistry, quantum-size-related properties, and applications toward biology, catalysis, and nanotechnology. Chem. Rev. 104, 293–346. https://doi.org/10.1021/cr030698+.

Liz-Marzán, L.M., 2006. Tailoring surface plasmons through the morphology and assembly of metal nanoparticles. Langmuir 22, 32–41. https://doi.org/10.1021/la0513353.

Kochuveedu, S.T., Kim, D.-P., Kim, D.H., 2012. Surface-plasmon-induced visible light photocatalytic activity of TiO2 nanospheres decorated by Au nanoparticles with controlled configuration. J. Phys. Chem. C. 116, 2500–2506. https://doi.org/10.1021/jp209520m.

Oros-Ruiz, S., Pedraza-Avella, J.A., Guzmán, C., Quintana, M., Moctezuma, E., del Angel, G., Gómez, R., Pérez, E., 2011. Effect of gold particle size and deposition method on the photodegradation of 4-chlorophenol by Au/TiO2. Top. Catal. 54, 519–526. https://doi.org/10.1007/s11244-011-9616-y.

Murdoch, M., Waterhouse, G.I., Nadeem, M.A., Metson, J.B., Keane, M.A., Howe, R.F., Llorca, J., Idriss, H., 2011. The effect of gold loading and particle size on photocatalytic hydrogen production from ethanol over Au/TiO2 nanoparticles. Nat. Chem. 3, 489–492. https://doi.org/10.1038/nchem.1048.

Li, A., Zhang, P., Chang, X., Cai, W., Wang, T., Gong, J., 2015. Gold Nanorod@TiO2 yolk-shell nanostructures for visible-light-driven photocatalytic oxidation of benzyl alcohol. Small. 11, 1892–1899. https://doi.org/10.1002/smll.201403058.

Hu, C., Zhang, X., Li, X., Yan, Y., Xi, G., Yang, H., Bai, H., 2014. Au photosensitized TiO2 ultrathin nanosheets with 001 exposed facets. Chemistry. 20, 13557–13560. https://doi.org/10.1002/chem.201403428.

Kodiyath, R., Manikandan, M., Liu, L., Ramesh, G.V., Koyasu, S., Miyauchi, M., Sakuma, Y., Tanabe, T., Gunji, T., Duy Dao, T., Ueda, S., Nagao, T., Ye, J., Abe, H., 2014. Visible-light photodecomposition of acetaldehyde by TiO2-coated gold nanocages: plasmon-mediated hot electron transport via defect states. Chem. Commun. 50, 15553–15556. https://doi.org/10.1039/c4cc06229a.

Alvarez-Puebla, R., Liz-Marzán, L.M., García de Abajo, F.J., Light, F.J., 2010. Light Concentration at the nanometer scale. J. Phys. Chem. Lett. 1, 2428–2434. https://doi.org/10.1021/jz100820m.

Stöber, W., Fink, A., Bohn, E., 1968. Controlled growth of monodisperse silica spheres in the micron size range. J. Colloid Interf. Sci. 26, 62–69. https://doi.org/10.1016/0021-9797(68)90272-5.

Sclafani, A., Herrmann, J.M., 1996. Comparison of the photoelectronic and photocatalytic activities of various anatase and rutile forms of Titania in pure liquid organic phases and in aqueous solutions. J. Phys. Chem. 100, 13655–13661. https://doi.org/10.1021/jp9533584.

Xu, M., Gao, Y., Moreno, E.M., Kunst, M., Muhler, M., Wang, Y., Idriss, H., Wöll, C., 2011. Photocatalytic activity of bulk TiO2 anatase and rutile single crystals using infrared absorption spectroscopy. Phys. Rev. Lett. 106,. https://doi.org/10.1103/PhysRevLett.106.138302 138302.

Zuber, A., Purdey, M., Schartner, E., Forbes, C., van der Hoek, B., Giles, D., Abell, A., Monro, T., Ebendorff-Heidepriem, H., 2016. Detection of gold nanoparticles with

different sizes using absorption and fluorescence based method. Sens. Actuators B. 227, 117–127. https://doi.org/10.1016/j.snb.2015.12.044.
Kaur, H., Kumar, S., Verma, N.K., Singh, P., 2018. Role of pH on the photocatalytic activity of TiO_2 tailored by W/T mole ratio. J. Mater. Sci. Mater. Electron. 29, 16120–16135. https://doi.org/10.1007/s10854-018-9701-0.
Tedstone, A.A., Lewis, D.J., O'Brien, P.O., 2016. Synthesis, properties and applications of transition metal-doped layered transition metal dichalcogenides. Chem. Mater. 28, 1965–1974. https://doi.org/10.1021/acs.chemmater.6b00430.
He, C., Cheng, M., Zhang, W.X., 2018. Tunable electronic and magnetic properties of transition metals doped antimonene: a first-principles study. Mater. Res. Exp. 5. https://doi.org/10.1088/2053-1591/aacdd7.
Lkhagvadulam, B., Kim, J.H., Yoon, I., Shim, Y.K., 2013. Photodynamic activity of gold nanoparticles conjugate of water soluble purpurin-18-N-methyl-D-glucamine. BioMed Res. Int., 720759 https://doi.org/10.1155/2013/720579.
Atif, M., Iqbal, S., Fakhar-E-Alam, M., Ismail, M., Mansoor, Q., Mughal, L., Aziz, M.H., Hanif, A., Farooq, W.A., 2019. Manganese-doped cerium oxide nanocomposite induced photodynamic therapy in MCF-7 cancer cells and antibacterial activity. BioMed Res. Int. 2019, 1–13. https://doi.org/10.1155/2019/7156828.
Iqbal, S., Fakhar-e-Alam, M., Atif, M., Amin, N., Alimgeer, K.S., Ali, A., Aqrab-ul-Ahmad, Hanif, A., Aslam Farooq, W., 2019. Structural, morphological, antimicrobial, and in vitro photodynamic therapeutic assessments of novel Zn + 2-substituted cobalt ferrite nanoparticles. Results Phys. 15. DOI: 10.1016/j.rinp.2019.102529, http://www.ncbi.nlm.nih.gov/pubmed/102529.
Iqbal, S., Fakhar-e-Alam, M., Akbar, F., Shafiq, M., Atif, M., Amin, N., Ismail, M., Hanif, A., Farooq, W.A., 2019bb. Application of silver oxide nanoparticles for the treatment of cancer. J. Mol. Struct. 1189, 203–209. https://doi.org/10.1016/j.molstruc.2019.04.041.
Fakhar-e-Alam, M., Aqrab-ul-Ahmad, Atif, M., Alimgeer, K.S., Suleman Rana, M., Yaqub, N., Aslam Farooq, W., Ahmad, H., 2020. Synergistic effect of TEMPO-coated TiO2 nanorods for PDT applications in MCF-7 cell line model. Saudi J. Biol. Sci.. DOI: 10.1016/j.sjbs.2020.09.027.
S. Iqbal, S., Fakhar-e-Alam, M., Atif, M., Ahmed, N., -ul-Ahmad, A., Amin, N., Alghamdi, R., Hanif, A., Farooq, W., 2019. Empirical modeling of Zn/ZnO nanoparticles decorated/conjugated with fotolon (chlorine e6) based photodynamic therapy towards liver cancer treatment. Micromachines. 10, 60. DOI: 10.3390/mi10010060.
Kovacs, G., ZsoltPap, C. Cotet, Veronica, C., 2015. Lucian Baia and V. Danciu, photocatalytic, morphological and structural properties of the TiO2-SiO2-Ag porous structures based system. Materials. 8, 1059–1073. https://doi.org/10.3390/ma8031059.
Xu, J., Sun, Y., Zhao, Y., Huang, J., Chen, C., Jiang, Z. Photocatalytic inactivation effect of gold-doped TiO2 (Au/TiO2) nanocomposites on human colon carcinoma LoVo cells; Hindawi publishing corporation. Int. J. Photoenergy Volume (2007), 1-7, Article ID 97308. DOI: 10.1155/2007/97308.
Moosavi, M.A., Sharifi, M., Ghafary, S.M. Zahra M. A. p., Alireza K., Marvesh R., Sadaf H., Marek J. L., Thomas K., Saeid G., 2016. Photodynamic N-TiO2 nanoparticle treatment induces controlled ros-mediated autophagy and terminal differentiation of leukemia cells, Sci. Rep.
Tisdale, W.A., Williams, K.J., Timp, B.A., Norris, D.J., Aydil, E.S., Zhu, X.-Y., 2010. Hot-electron transfer from semiconductor nanocrystals. Science. 328, 1543–1547. https://doi.org/10.1126/science.1185509.
Clavero, C., 2014. Plasmon-induced hot-electron generation at nanoparticle/metal-oxide interfaces for photovoltaic and photocatalytic devices. Nat. Photonics. 8, 95–103. https://doi.org/10.1038/nphoton.2013.238.
Qiu, H., Tan, M., Ohulchanskyy, T.Y., Lovell, J.F., Chen, Guanying, 2018. Recent progress in Upconverstion photodynamic therapy. Nanomaterials. 8, 344. https://doi.org/10.3390/nano8050344.
Atif, M., Devanesan, S., AlSalhi, M.S., Masilamani, V., Saleem, M.N.A., AlShebly, M., Farhat, K., Hussain, I., Alimgeer, K.S., 2020. An experimental and algorithm-based study of the spectral features of breast cancer patients by a photodiagnosis approach. Photodiagn. Photodyn. Ther. 31,. https://doi.org/10.1016/j.pdpdt.2020.101851 101851.
Atif, M., Fakhar-e-Alam, M., Abbas, N., Siddiqui, M. A., Ansari, A. A., Al-Khedhairy, A. A., Wang, Z. M., 2016. In vitro cytotoxicity of mesoporous SiO2@Eu(OH)3 core-shell nanospheres in MCF-7, Hindawi. J. Nanomater. 6, Article ID 7691861.
Iqbal, S., Fakhar-e-Alam, M., Atif, M., Amin, N., Ali, A., Shafiq, M., Ismail, M., Hanif, A., Farooq, W.A., 2020. Photodynamic therapy, facile synthesis, and effect of sintering temperature on the structure, morphology, optical properties, and anticancer activity of Co3O4 nanocrystalline materials in the HepG2 cell line. J. Photochem. Photobiol. A. 386. https://doi.org/10.1016/j.jphotochem.2019.112130.